Functional Tuning of Photoactive Yellow Protein by Active Site Residue 46[†]

Andrew F. Philip,[‡] Kaury T. Eisenman,[‡] George A. Papadantonakis,[‡] and Wouter D. Hoff*[,§]

Department of Biochemistry and Molecular Biology, The University of Chicago, Chicago, Illinois 60637, and Department of Microbiology and Molecular Genetics, Oklahoma State University, Stillwater, Oklahoma 74078

Received September 10, 2008; Revised Manuscript Received October 28, 2008

ABSTRACT: Protein−ligand interactions alter the properties of active site groups to achieve specific biological functions. The active site of photoactive yellow protein (PYP) provides a model system for studying such functional tuning. PYP is a small bacterial photoreceptor with photochemistry based on its *p*-coumaric acid (pCA) chromophore. The absorbance maximum and pK_a of the pCA in the active site of native PYP are shifted from 400 nm and 8.8 in water to 446 nm and 2.8 in the native protein milieu, respectively, by protein−ligand interactions. We report high-throughput microscale methods for the purification and spectroscopic investigation of PYP and use these to examine the role of active site residue Glu46 in PYP, which is hydrogen bonded to the pCA anion. The functional and structural attributes of the 19 substitution mutants of PYP at critical active site position 46 vary widely, with absorbance maxima from 441 to 478 nm, pCA fluorescence quantum yields from 0.19 to 1.4%, pCA pK_a values from 3.0 to 9.0, and protein folding stabilities from 6.5 to 12.9 kcal/mol. The kinetics of the last photocycle transition vary by more than 4 orders of magnitude and are often strongly biphasic. Only E46Q PYP exhibits a greatly accelerated photocycling rate. All substitutions yield a folded, photoactive PYP, illustrating the robustness of protein structure and function. Correlations between side chain and mutant properties establish the importance of residue 46 in tuning the function of PYP and the significance of the strength of its hydrogen bond to the pCA. Native PYP exhibits the lowest values for pCA fluorescence quantum yield and pK_a, indicating their functional relevance. These results demonstrate the value of quantitative high-throughput biophysical studies of proteins.

Photoactive yellow protein (PYP)[1] from *Halorhodospira halophila* is a cytosolic photoreceptor (*1, 2*) that mediates the host organism's negative phototaxis in response to blue light (*3*). The biochemical and biophysical properties of PYP have been studied extensively (*4*−*6*) due to the rich biophysics of its light-triggered function and its extraordinary ease of handling, including its solubility (*1*), thermostability (*2*), and excellent overexpression in *Escherichia coli* (*7, 8*). The protein interacts with light via a *p*-coumaric acid (pCA) chromophore covalently bound to Cys69 (*9, 10*). Absorption of a photon by the initial pG state of PYP causes pCA *trans*−*cis* isomerization that triggers a complex photocycle (*2, 11*), resulting in the formation a photoactivated state, pB, that presumably has a downstream effect on cell motility. In the pG state, the pCA is deprotonated and in the *trans* conformation (*10, 12*). At neutral pH, the pB state decays back to the initial pG state in approximately 250 ms (*2, 8, 11*).

The crystal structure of PYP (*13*) provides detailed information about the side chains interacting with the pCA chromophore (Figure 1). The side chains Glu46 and Tyr42 form hydrogen bonds to the phenolic oxygen of the pCA, thus stabilizing its buried charge. Mutagenesis of Glu46 and Tyr42 significantly alters the properties of PYP, confirming the importance of these two side chains. Residue 46 is known to be involved in tuning the absorbance maximum (λ_{max}) and pK_a of the pCA chromophore, and the photocycle kinetics in PYP, based on studies of the E46Q, E46A, and E46D mutants (*8, 14*−*16*). In addition, it has a very short hydrogen bond to the pCA (*17*) (Figure 1b), has been identified as the proton donor for the ionized pCA during the PYP photocycle (*18*−*20*), and has been uncovered as a key factor in triggering protein conformational changes upon pB formation (*18, 20, 21*). The importance of Glu46 is also supported by the high degree of conservation of this residue within the PYP family of proteins (*7, 22*).

The properties of the pCA chromophore in PYP are greatly shifted compared to their values in water. In solution, pCA has a λ_{max} at 286 nm (at neutral pH) and a pK_a of 8.8 (*10, 23*). Within PYP, the pCA has its λ_{max} shifted to 446 nm and its pK_a shifted to 2.8 (*1, 24, 25*). In addition, the photochemical quantum yield is high (approximately 50%) (*26, 27*), while its fluorescence quantum yield is low (0.19%) (*28*), indicating that the PYP binding pocket promotes photochemistry over fluorescence. These tuning phenomena illustrate a common

[†] W.D.H. gratefully acknowledges support from NIH Grant GM063805 and OCAST Grant HR07-135S.

* To whom correspondence should be addressed. Telephone: (405) 744-4449. Fax: (405) 744-6790. E-mail: wouter.hoff@okstate.edu.

[‡] The University of Chicago.

[§] Oklahoma State University.

[1] Abbreviations: λ_{max}, absorbance maximum; Φ_{fl}, fluorescence quantum yield; E46Q^{Ht}, mutant of His-tagged PYP in which Glu46 is substituted with glutamine; E46X, library of 20 PYP derivatives in which residue 46 is substituted with each of the 20 side chains; $\Delta G°_U$, free energy difference between the folded and unfolded state; Gdm-HCl, guanidinium hydrochloride; pB, blue-shifted long-lived photocycle intermediate; pB$_{dark}$, blue-shifted acid-denatured state of PYP; pCA, *p*-coumaric acid; PYP, photoactive yellow protein; pG, ground state of PYP; wtPYP^{nHt}, wild-type PYP without a His tag.

10.1021/bi801730y CCC: $40.75
Published on Web 12/08/2008

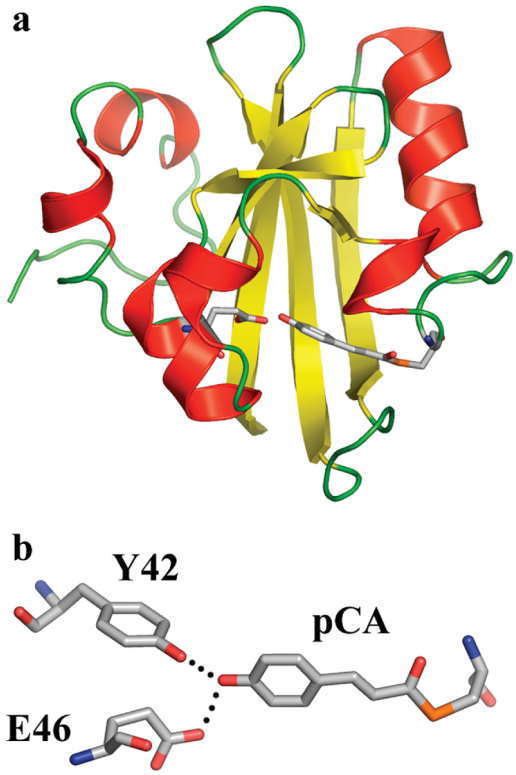

FIGURE 1: Structure of PYP and its pCA chromophore. Schematic illustration of the crystal structure of PYP (helices colored red, sheets yellow, and loop regions green) (a) and active site of PYP with Glu46 and Tyr42 hydrogen bonded to the pCA (b).

property of proteins in general: ligands or amino acid residues within the protein have their chemical properties adjusted with the aim of accomplishing a biochemical goal. In the case of PYP, the color is tuned to make the protein sensitive to a specific wavelength regime. The pCA pK_a is tuned to facilitate a proton transfer switch coupled to protein conformational changes. In the dark state of PYP, the pK_a values of Glu46 and the pCA are such that the pCA remains protonated; photoexcitation of PYP triggers transfer of a proton from Glu46 to the pCA, causing receptor activation (*18, 20*). Acid denaturation of PYP also results in pCA protonation and the formation of the blue-shifted state (*1, 25*), pB_{dark}, allowing the apparent pK_a of the pCA to be determined. PYP offers a unique system with which to study biochemical tuning because it can conveniently be activated and observed using light. Here we describe methods for the purification of PYP in 96-well format and use this to study the effects of all 19 substitutions at position 46 on the protein−ligand interaction between PYP and its pCA chromophore using high-throughput methods.

MATERIALS AND METHODS

Mutagenesis. Mutagenesis was performed using Stratagene's QuikChange site-directed mutagenesis kit with primers degenerate at position 46 (5′-ATC CTT CAG TAC AAC GCC GCG NNN GGC GAC ATC ACC GGC CGC GAC-3′ and complement). A pQE-80A plasmid (Qiagen) containing the *pyp* gene inserted between *Bam*HI and *Hin*dIII sites was used as a template. The PCR products were digested with *Dpn*I and transformed into *E. coli* DH5α. Transformants were grown overnight in liquid culture to resolve mismatches at position 46 during in vivo replication. DNA was then purified using a QIAPrep Spin Miniprep kit (Qiagen) and transformed into *E. coli* BL21 cells grown on LB agar with ampicillin (200 μg/mL). Protein samples were purified as described below, and the individual mutants were separated on the basis of their unique absorbance spectra.

Expression and Purification of PYP in 96-Well Microplates. Colonies were picked and inoculated into deep-well microplates containing 0.5 mL of Terrific Broth per well with 200 μg/mL ampicillin and handled using a procedure adapted from ref *29* (also see Methods in the Supporting Information). The microplates were covered with gas-permeable adhesive covers (ABGene catalog no. AB-0718) and grown overnight on a microplate shaker operating inside a 37 °C incubator. The next day, 100 μL of the overnight cultures was used to inoculate expression cultures (deep-well microplates containing 1.2 mL of Terrific Broth per well with ampicillin), and freezer stocks were prepared from 140 μL of culture and 60 μL of glycerol stored at −80 °C in a freezer-safe microplate. After growth for 1.5 h, IPTG was added (final concentration of 1 mM) to the expression cultures, and growth was continued for 4−5 h. The cells were pelleted using a centrifuge equipped with microplate holders (2800*g* for 30 min).

The cells were frozen, thawed, and lysed using 200 μg/mL lysozyme and 0.5 μg/mL DNase I. PYP was reconstituted using pCA anhydride (*30*). After centrifugation, the soluble fractions were pipetted into GF/C filter plates (Whatman catalog no. 7700-3301) stacked on top of polypropylene filter plates (Whatman catalog no. 7700-3305) containing 40 μL of Ni-NTA agarose (QIAGEN) per well and sealed on the bottom with Parafilm. The soluble cell extract was centrifuged into the polypropylene plates. The resin was washed by centrifugation using a denaturing wash step [100 mM sodium phosphate, 10 mM Tris-HCl, and 6 M guanidine HCl (pH 8.0)] followed by three washes with lysis buffer [50 mM sodium phosphate, 500 mM NaCl, and 10% glycerol (pH 8.0)], and one wash with elution buffer lacking EDTA. Protein was eluted from the resin by incubation for 30 min with 200 μL of elution buffer containing 50 mM EDTA and centrifugation into a collection plate. The precise composition of the elution buffer depended on the desired pH. All of the elution buffers contained 100 mM NaCl and 50 mM EDTA. For pH 8.0, the buffering agent was 20 mM Tris-HCl, and for pH 9.0 or 9.5, it was 20 mM CHES.

Data Collection. Absorbance spectra were measured in either a Synergy HT plate reader (Bio-Tek) or individually with a microcuvette in a Hewlett-Packard (now Agilent Technologies) 8453 UV−vis spectrophotometer. Fluorescence spectra were measured individually in a SPEX Fluoromax-3 fluorometer (Jobin-Yvon) using a 100 μL fluorescence microcuvette (also see Methods in the Supporting Information). Fluorescence was excited at 445 nm and detected from 465 to 600 nm. To compare the fluorescence quantum yields of the mutants with those of wtPYP, the emission spectra obtained for samples with identical optical densities at 445 nm were integrated from 465 to 600 nm.

For pH titrations, a dip probe and fiber-optic coupler (Custom Sensors&Technology) were used to convert the 8453 spectrophotometer into a device capable of taking measurements within a microplate well. A square-well microplate (Whatman catalog no. 7701-1651) was used to

accommodate the dip probe as well as a micro-pH electrode (Thermo Orion catalog no. 9803BN) and a small stir bar. In this manner, acid/base could be manually titrated and absorbance and pH measurements acquired simultaneously. Dilution effects were taken into account.

Protein stability was measured by chemical denaturation using buffer with 8 M guanidine hydrochloride. Samples in 96-well plates were titrated using a 12-channel pipetter, and absorbance measurements were taken in the Synergy HT plate reader. Plates with flat-bottom wells were used so that changes in volume were directly proportional to changes in path length. Thus, no corrections were needed for dilution effects.

Dark-state recovery kinetics were recorded with the 8453 spectrophotometer with the sample in a microcuvette. Actinic light from a 150 W halogen lamp (Cuda model I-150) was directed onto the sample through the top of the cuvette using a fiber-optic light guide. The sample was illuminated for approximately 30 s before the light source was shuttered and the recovery of the pG dark-state absorbance was monitored with a time resolution of 100 ms.

All measurements taken in a cuvette (with the 8453 spectrophotometer or the Fluoromax-3 fluorometer) were performed at 25 °C. All other measurements were taken at room temperature. Absorbance and fluorescence spectra were measured from samples at pH 9.5 to minimize the amounts of acid-denatured species. All other samples were at pH 8.0.

Data Analysis. Titration curves were fit with a sigmoidal relationship derived from the Henderson−Hasselbalch equation. The equation was modified to include sloping baselines, as well as an *n* value that accounts for variations in the steepness of the transition (*31*) (eq 1)

$$A = \{a_u + b_u \times \mathrm{pH} + (a_l + b_l \times \mathrm{pH})[10^{n(\mathrm{p}K_a - \mathrm{pH})}]\}/[1 + 10^{n(\mathrm{p}K_a - \mathrm{pH})}] \quad (1)$$

The parameters *a* and *b* are the *y*-intercept and slope of each baseline, respectively. The subscripts u and l denote the terms for the upper and lower baselines, respectively. The pK_a is the pH value at which half of the sample is ionized.

Denaturant titration data were fit with a sigmoidal relationship with sloping baselines (*32*) (eq 2)

$$y = \left[a_u + b_u \times [\mathrm{D}] + (a_l + b_l \times [\mathrm{D}]) \times \exp\left(\frac{-\Delta G^\circ + m[\mathrm{D}]}{RT}\right)\right] \Big/ \left[1 + \exp\left(\frac{-\Delta G^\circ + m[\mathrm{D}]}{RT}\right)\right] \quad (2)$$

The pG dark-state recovery traces were fit with the sum of two exponential rise functions (eq 3)

$$y = y_0 + a[1 - \exp(-bt)] + c[1 - \exp(-dt)] \quad (3)$$

The parameter y_0 indicates the minimum value from which the recovery starts. The parameters *a* and *c* indicate the amplitudes of the two rate constants *b* and *d*.

RESULTS

Ninety-Six-Well Expression and Purification of PYP. To allow the application of 96-well approaches to the study of PYP, its expression and purification in 96-well plates were examined. The method is based on the His_6 tag extension at the N-terminus of PYP (modified slightly from ref *29*) that allows a one-step purification using Ni-NTA resin. This procedure reproducibly yielded ∼100−200 μg of PYP per well in 96-well format with high purity, as shown by SDS−PAGE and purity index (typically ∼0.60) (Figure S1 of the Supporting Information). In comparison, a multistep purification from a 1 L culture typically yields ∼30 mg of PYP with a purity index of ≤0.48 (*18*). The one-step 96-well purification procedure yields samples in which an estimated 75−85% of the protein is PYP with an N-terminal His_6 affinity tag ($MRGSH_6GSD_4K$). Below, comparisons between mutants and wtPYP are made with both having His_6 tags. When PYP without a His_6 tag is referenced below, it will be denoted as PYP^{nHt}.

To test the applicability and value of 96-well approaches to biophysical studies of proteins, we characterized the complete set of 20 proteins in the E46X library with respect to a number of functional properties: pCA λ_{max}, fluorescence quantum yield Φ_{fl}, and pK_a, free energy for unfolding ΔG°_U, and photocycle pG recovery kinetics. In these experiments, methods that are fully compatible with high-throughput techniques were used.

Absorbance Spectra of the E46X Mutants. A monochromator-based plate reader was used to acquire complete absorbance spectra of the 20 proteins in the E46X library. This allowed the measurement of 96 absorbance spectra (260−600 nm) in ∼90 min with a spectral quality (±1 nm) that is only slightly lower than that obtained with a traditional cuvette-loaded spectrophotometer.

All 19 mutants yielded a protein with a visible absorbance band (Figure 2a). On the basis of the absorbance at the peak of the visible absorbance band, the samples had purification yields that are similar to that for wtPYP, within a factor of 2. Even at pH 9.5, some of the mutants exhibit an absorbance band near 350 nm, indicating that the pCA is partially protonated due to a greatly upshifted pK_a (as confirmed below). To allow direct comparison of the absorbance bands of the ionized pCA in the mutants, the amplitudes of their absorbance spectra were normalized at their visible absorbance maxima. For mutants containing a significant amount of protonated pCA, this normalization increases their relative concentration in Figure 2a. This explains most of the variation in the amplitude of the 280 nm absorbance bands of the mutants. The λ_{max} values of the pCA absorbance bands in the E46X library range from 441 nm (E46P) to 478 nm (E46I and E46V), compared to 446 nm for wtPYP (Figure 2b). A complete list of the properties of the E46X mutants reported here is provided in Table S1 of the Supporting Information. Most mutants have a red-shifted λ_{max}; only five mutants were shifted to the blue (Figure 2b). Also, the extent of the observed red shifts (up to 32 nm) was larger than that of the blue shifts (up to 5 nm). Substitutions with small hydrophobic residues resulted in the largest red shifts. Substitutions with proline and acidic/basic residues (except E46H) resulted in the strongest blue shifts.

Fluorescence Emission Quantum Yield. Emission spectra of the E46X library (data not shown) were recorded using integration times of both 0.1 and 0.5 s to test if excitation lamp-induced photocycling affects the results. No significant difference was noted (data not shown). The Φ_{fl} of the mutants was determined using the published value for $wtPYP^{nHT}$ of 0.14% (*28*) as a standard. Most of the mutants had Φ_{fl} values that fell within a narrow range (0.53−0.66) (Figure 3). The Q, M, and L substitutions had Φ_{fl} below this range, while

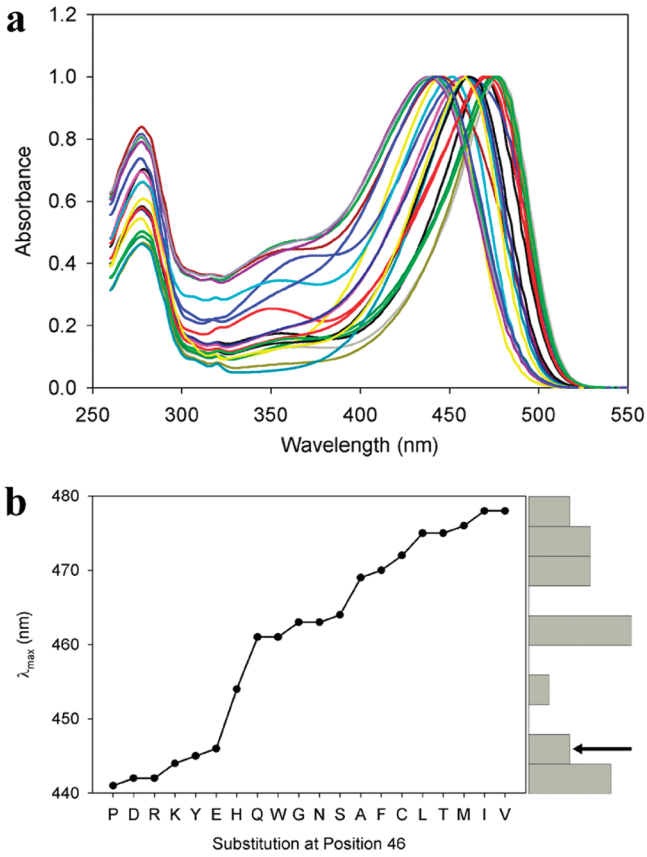

FIGURE 2: Absorbance spectra of the E46X PYP mutants. (a) Normalized absorbance spectra of the E46X library at pH 9.5. (b) Dependence of the visible absorbance maximum λ_{max} on the substitution at position 46. Substitutions were sorted from most blue-shifted to most red-shifted. A histogram of the distribution is shown on the right axis. The location of wtPYP is indicated by an arrow.

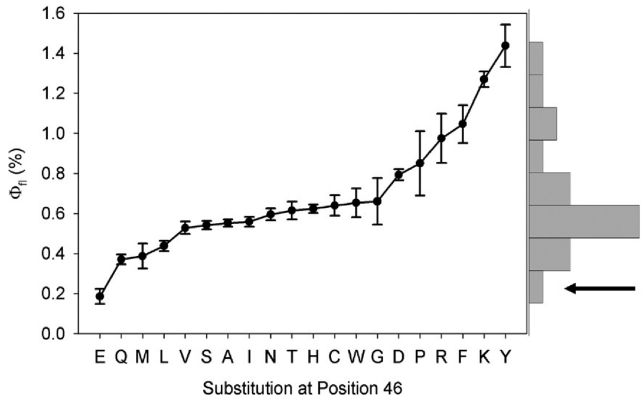

FIGURE 3: Quantum yield of pCA fluorescence Φ_{fl} in the E46X PYP mutants. The dependence of Φ_{fl} at pH 9.5 on the substitution at position 46 is shown. Substitutions were sorted from lowest to highest Φ_{fl}. The plot represents the average of two data sets measured using different integration times (0.1 and 0.5 s; see the text). Errors bars indicate one standard deviation. A histogram of the distribution within the library is shown on the right axis. The location of wtPYP is indicated by an arrow.

D, P, R, K, F, and Y had a higher Φ_{fl}. A notable observation is that all of the mutants exhibit a Φ_{fl} larger than that of wtPYP (0.19%), increased up to 7-fold (1.4%).

pH Titrations. Since the side chain of Glu46 is hydrogen bonded to the pCA, mutations at this residue can be expected to affect the pK_a of the pCA, as has already been shown for the E46Q, E46A, and E46D mutants (*8, 15, 16*). To systematically investigate this effect for all substitutions at this position, we performed pH titrations with visible absorbance monitoring in individual 96-well samples. Acid titration of PYP results in the protonation of the pCA chromophore, and a blue shift in the absorbance spectrum to ~350 nm. A typical data set is shown in Figure 4a. Such pH titration measurements were performed for all 20 samples in the E46X library (Figure 4b). The pH dependence of the absorbance at the pCA λ_{max} for each mutant was fit using eq 1 to determine the pK_a and slope n of the transition.

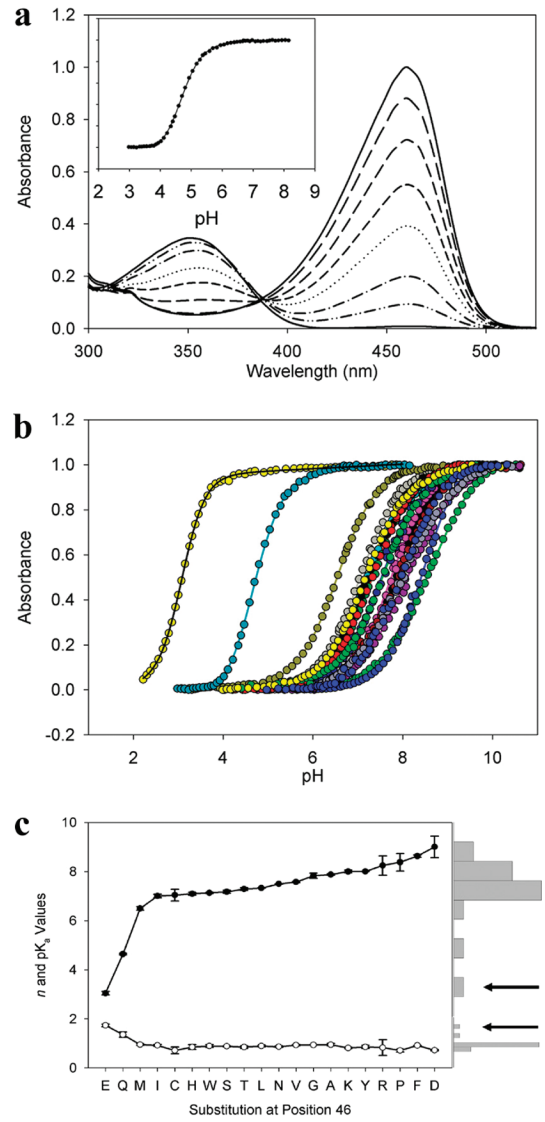

FIGURE 4: Dependence of absorbance spectra of the E46X PYP mutants on pH. (a) An example titration of the pH dependence of the absorbance spectrum (E46Q PYP). The data were thinned for clarity. The inset shows the titration curve at the absorbance maximum (461 nm) derived from the visible absorbance spectra. (b) Amplitude-normalized pH titration curves for the entire E46X library, measured at the absorbance maximum for each protein. The pH titrations were fit using eq 1. (c) Dependence of the pK_a (●) and n values (○) on the substitution at position 46. Substitutions were sorted from lowest to highest pK_a. Errors bars represent the standard deviation from the average of two measurements. Histograms of the distributions of pK_a and n values are shown on the right axis. The locations for wtPYP are indicated with arrows.

This revealed that the pK_a of the pCA varied by 6 pH units from 3.0 for wtPYP to 9.0 for the E46D mutant. Almost all of the mutants, in contrast with wtPYP, exhibit apparent pK_a values close to that of solvent-exposed pCA (Figure 4c).

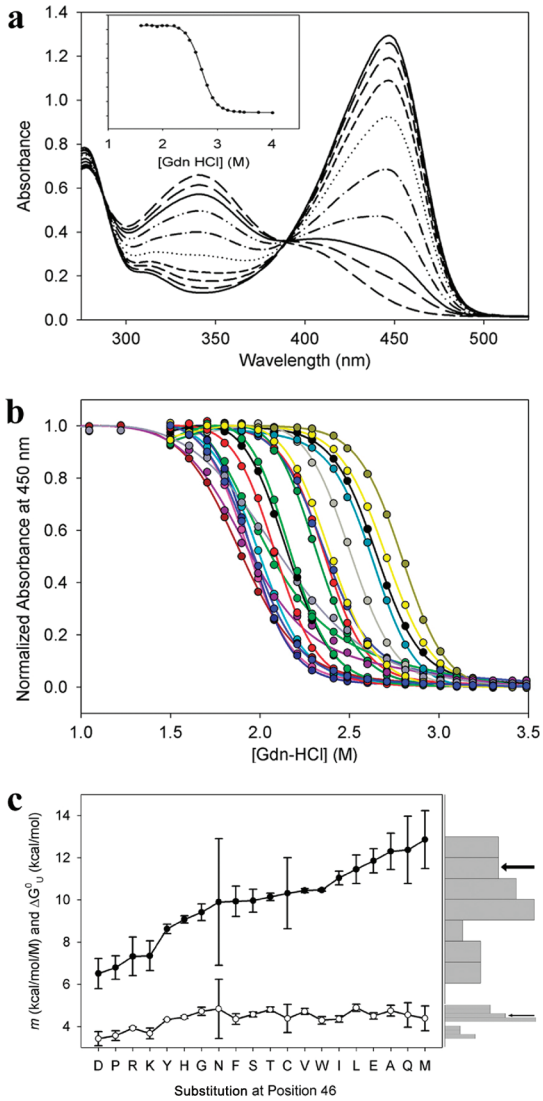

FIGURE 5: Denaturation of the E46X PYP mutants at pH 8.0 with Gdn-HCl. (a) Dependence of the absorbance spectrum of wtPYP on Gdn-HCl as an example denaturant titration. The inset shows the titration curve at 450 nm. (b) Gdn-HCl titrations for the entire E46X library. The denaturant titrations were fit using eq 2. (c) Dependence of the stability ΔG°_{Un} (●) and *m* values (○) on the substitution at position 46. Substitutions were sorted from lowest to highest ΔG°_{U}. Errors bars represent one standard deviation from the mean of a minimum of two measurements. Histograms of the distributions of ΔG°_{U} and *m* values are shown on the right axis. The locations of wtPYP are indicated by arrows.

The only exception is the conservative substitution E46Q which has an apparent pK_a of ~4.6, intermediate between that of wtPYP and those of the rest of the mutants.

The *n* values for most of the titration curves were close to 1, which would be expected for a single-site titration (Figure 4c). For wtPYP and E46Q, the *n* values are greater than 1, suggesting some degree of cooperativity. The *n* values for the C, D, K, P, and R substitutions were near 0.75 (see the Discussion in the Supporting Information).

Guanidine Titrations. The folding of PYP can be described with a two-state mechanism (*33*). In the folded state, the pCA absorbs in the visible region. In the unfolded state, the pCA absorbance is shifted to ~340 nm (*2*). Thus, the visible absorbance band of PYP can be used as an indicator of the folded−unfolded equilibrium (Figure 5a). Guanidine titrations were performed in 96-well plate format for all 20 members of the E46X library using visible detection (Figure 5b). The titration data were fit (*32*) using eq 2 to determine the *m* value and ΔG°_{U} (Figure 5c). The ΔG°_{U} values for the mutants varied from 6.5 kcal/mol for the E46D mutant to 12.9 kcal/mol for the E46M mutant. The majority of the mutants exhibit reduced ΔG°_{U} values, around 10 kcal/mol. Three mutants stand out as having stabilities that are higher than expected (see Discussion): E46A, E46M, and E46W.

The *m* values for most of the 20 samples are largely constant at 4.5 kcal mol^{-1} M^{-1} (Figure 5c). The E46D, E46K, E46P, and E46R mutants are exceptions with lower *m* values (near 3.7 kcal mol^{-1} M^{-1}). These same mutants also have the lowest ΔG°_{U} compared to that of wtPYP.

Dark-State Recovery Kinetics. All 19 mutants exhibited a light-induced photocycle with a blue-shifted photocycle intermediate. We measured the kinetics of the last photocycle transition in PYP, from the blue-shifted pB intermediate to the initial pG state for the E46X library at pH 8.0. In wtPYP^{nHt}, this step proceeds on the order of 0.2 s at pH 8.0 (*2, 8, 11*), with 5−10% of the population decaying 1 order of magnitude more slowly (*11*). Among the E46X mutants (with His tags), the recovery times vary more than 4 orders of magnitude: from tens of minutes to beyond the time resolution of the spectrophotometer (0.1 s) (Figure 6). Typically, the fastest were the mutants with small hydrophobic substitutions. The slowest were E46P and the acidic/basic substitutions (except E46H). Quantitative descriptions are complicated by the fact that different mutants exhibited different behaviors. Some recovery traces were fit well with single-exponential functions, while others (including wtPYP) required multiple exponentials (Figure S2 of the Supporting Information). For the 19 mutants, the relative contribution of the faster time constant varied from 15 to 100% (Figure 6c). To distill the data into a single metric that can be used to directly compare mutants, we determined the degree of steady-state bleaching given a fixed amount of light (same illumination conditions used for all measurements) (Figure 7).

Our photocycle measurements for E46Q PYP revealed a photocycle at pH 8.0 (0.6 s^{-1}) much slower than that reported in the literature [21 s^{-1} for E46Q^{Ht} (*34*) and 150 s^{-1} for E46Q^{nHt} (*8*)]. This issue was resolved by considering the very small fraction of photobleaching of E46Q (Figure 7). If the entire E46Q population would exhibit a pB to pG transition rate of 0.6 s^{-1}, then a much larger bleaching percentage would be expected (see the Discussion in the Supporting Information). We conclude that the majority of the population of the E46Q mutant proteins exhibits a rate of pG recovery beyond our time resolution, while a small fraction of the sample has a much slower recovery rate.

To investigate if other mutants also exhibit photocycle kinetics with a major component faster than the 100 ms time resolution of the spectrophotometer used here, we compared the measured photobleaching percentage with the photobleaching percentage calculated on the basis of the observed recovery rates, assuming parallel pathways (see Figure S3 of the Supporting Information) in the case of mutants with a biphasic recovery rate (see the Discussion in the Supporting Information). Only in the case of the E46Q mutant was a clear discrepancy found between the observed and expected percentage of photobleaching (Figure S3 of the Supporting

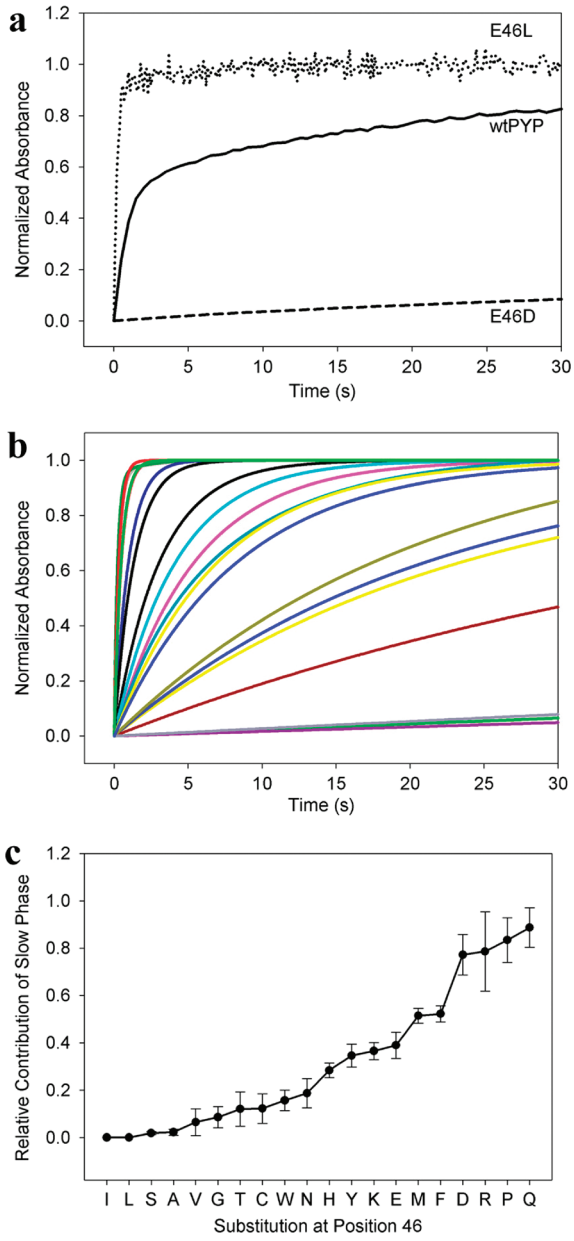

FIGURE 6: Kinetics of the final photocycle transition in the E46X PYP mutants at pH 8.0. (a) Normalized examples of dark-state recovery traces. Data for wild-type PYP (—), the fast mutant E46L (•••), and the slow mutant E46D (---) are shown, detected at their visible absorbance maxima (446, 475, and 442 nm, respectively). (b) Biexponential fits using eq 3 of the amplitude-normalized kinetics of the pB → pG photocycle recovery in the mutants. (c) Dependence of the relative contribution to the slow phase in pG recovery kinetics on the substitution at position 46. Substitutions were sorted from lowest to highest percentage of slow pG recovery phase.

Information). On the basis of this, we conclude that only the E46Q mutant exhibits a recovery rate much faster than 10 s^{-1} of the mutants in the E46X library.

DISCUSSION

Implications for the Mechanism of Spectral Tuning and pK_a Tuning in PYP. The relationship between the structure of a protein and its function is a central unresolved problem in biology. In particular, questions remain regarding the mechanisms involved in the tuning of the properties of active sites and their cofactors to achieve spectacular rate enhancements and specific biological functions. To study these questions, we utilized active site residue Glu46 in PYP.

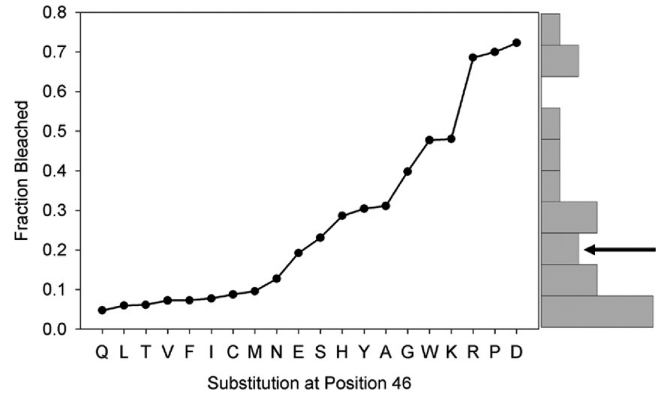

FIGURE 7: Dependence on the substitution at position 46 of the fraction of photobleached PYP after illumination for 30 s at pH 8.0. Substitutions were sorted from lowest to highest fraction bleaching. A histogram of the distribution of bleaching fraction is shown on the right axis. The location of wtPYP is indicated by an arrow.

The E46Q substitution lengthens, and presumably weakens, the hydrogen bond with the pCA by 0.29−0.35 Å (*17, 35*) and leads to a shift of the λ_{max} from 446 to 461 nm (*8, 14*). It has been proposed that the reduced charge localization caused by the weakening of this hydrogen bond results in the observed red shift in pCA λ_{max} (*8*) (also see the Discussion in the Supporting Information). When we replaced E with I, L, or V, residues with similar volumes but no hydrogen bonding capability, we observed an even further red shift to ~475 nm. This confirms the importance of the strength of the hydrogen bond between residue 46 and the pCA in the spectral tuning of PYP: progressive weakening of this hydrogen bond results in a progressive red shift of the λ_{max} (Figure 8a).

The absorbance spectrum of the E46W mutant initially was surprising in that it is very similar to that of E46Q (Figure 8b). On the basis of this observation, we propose that the NH group in the Trp side chain forms a hydrogen bond with the pCA similar to that with the Gln side chain (see the inset of Figure 8b). This is in line with the $\Delta G°_U$ of the E46W mutant (see below). However, in contrast to Gln46, the apparent hydrogen bond between Trp46 and the pCA apparently is not able to substantially lower the pK_a of the pCA (see Figure 4c). The hydrogen bonding status for the remaining substitutions remains to be determined (see the Discussion in the Supporting Information).

The data reported here indicate that the pK_a value of the pCA in PYP also depends on the strength of the hydrogen bond between residue 46 and the pCA. A combination of published data (*1, 8, 16, 25*) and the results reported here yields the following view. For wtPYP (strong hydrogen bond), the pK_a value is ~3; in the E46Q mutant (weakened hydrogen bond), it is shifted to ~5, and for the E46I, -L, and -V mutants (hydrogen bond absent), it is increased to ~7.5. This supports the notion that the hydrogen bond between residue 46 and the pCA stabilizes the ionized state of the pCA. However, when all 20 E46X samples are taken into consideration, no correlation is observed between the λ_{max} and the pK_a value of the pCA (Table 1). This indicates that additional factors are important for tuning these two

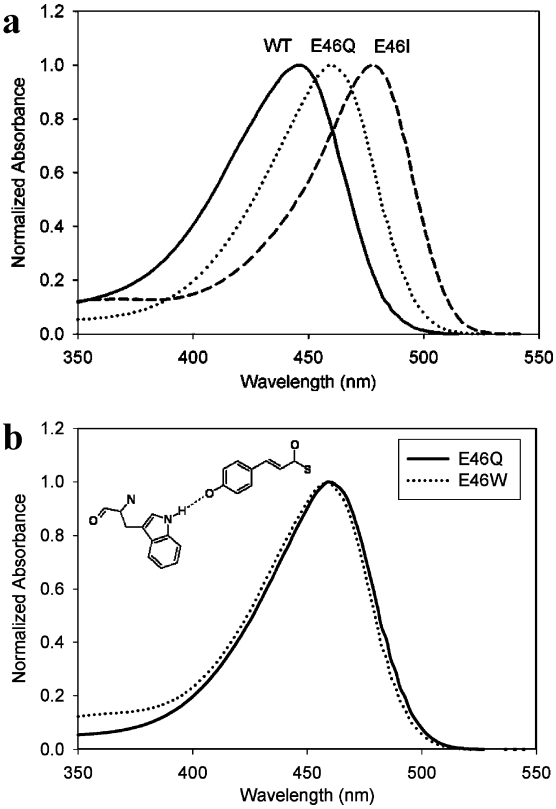

FIGURE 8: Spectral tuning in PYP by the hydrogen bond between the pCA chromophore and residue 46. (a) The absorbance spectra show a progressive red shift upon weakening and elimination of the hydrogen bond through wtPYP (—), E46Q (•••), and E46I (---). (b) E46Q (—) and E46W (•••) have very similar absorbance spectra, indicating the presence of a hydrogen bond between Trp46 and the pCA, as indicated in the inset.

Table 1: Correlation Coefficients for the Properties Determined for the 20 Proteins in the E46X Library[a]

	λ_{max}	pK_a	n	$\Delta G°_U$	m	Φ_{fl}	bleach
λ_{max}	1	0.086	0.029	−0.708	−0.721	0.488	0.797
pK_a	0.086	1	−0.896	−0.648	−0.362	0.662	0.455
n	0.029	−0.896	1	0.571	0.322	−0.534	−0.342
$\Delta G°_U$	−0.708	−0.648	0.571	1	0.743	−0.712	−0.775
m	−0.721	−0.362	0.322	0.743	1	−0.521	−0.782
Φ_{fl}	0.488	0.662	−0.534	−0.712	−0.521	1	0.452
bleach	0.797	0.455	−0.342	0.775	0.782	0.452	1

[a] Underlined values are significant to the 0.01 level.

functional properties that are differentially modified by mutations at position 46.

Both in the data reported here and in previous work, the n value for the acid denaturation of wtPYP is fractional and larger than 1 (Figure 4c and ref *25*). This apparent cooperativity in the acid denaturation of PYP remains unexplained. We found that the pCA pK_a and n value are correlated (Table 1) and that the only mutants in the E46X library with an n value of >1 are wtPYP and E46Q. These are also the only mutants with a low pK_a. On the basis of this observation, we propose that the cooperativity is based on the concomitant titration of the pCA and Asp/Glu side chains.

The pCA Φ_{fl} is a third property that is progressively increased when the hydrogen bond between residue 46 and the pCA in the E46Q and E46I, -L, and -V mutants is weakened. This suggests that increased mobility of the pCA within its protein binding pocket in the absence of a hydrogen bond tether causes the increased fluorescence emission.

Robustness and Evolvability of Protein Function. The side chain of Glu46 is fully buried within the active site of PYP, directly hydrogen bonded to the pCA (*13, 17*), and functionally important (*8, 14*−*16, 18*−*21, 36*). Despite its central importance, we found that all 19 substitutions of E46, including Gly and Trp, yielded a colored protein with photochemical activity. This indicates that the structure of PYP remains largely intact in the set of mutants studied here. Thus, the functional properties of PYP appear to be quite robust to active site perturbations. We conclude that the structure of PYP has sufficient flexibility to accommodate significant perturbations at its active site while maintaining its overall fold and many aspects of its functionality (see ref *37*). However, the values for various functional properties are significantly perturbed in the mutants. The observation that substitutions at functionally important active site residues alter function without abolishing it appears to be more general for proteins (*38*).

Functional Diversity from a Single Side Chain. We find here that different substitutions at position 46 of PYP result in a very significant variety of functional properties. Of note is where the properties of wtPYP fall within the ranges observed for the E46X library. While its λ_{max} (Figure 2b), $\Delta G°_U$ (Figure 5c), and dark-state recovery rate (Figure 7) are intermediate among those of the E46X library, the pCA Φ_{fl} (Figure 3) and particularly the pCA pK_a (Figure 4c) in wtPYP are significantly lower than those of the 19 mutants. This result suggests that the low Φ_{fl} and pK_a of the pCA have been selected for during evolution and are functionally important. The biological relevance of the low Φ_{fl} can be rationalized by evolutionary pressure to optimize the sensitivity of a photoreceptor, favoring a high quantum yield for photochemistry and thus a low Φ_{fl}. The unusually low pK_a of the pCA can be rationalized on the basis of the mechanism for receptor activation that has been described for PYP (*18, 20*). In this mechanism, proton transfer from the side chain of Glu46 to the pCA creates a destabilizing buried charge on Glu46 that acts as an "electrostatic epicenter" and drives protein conformational changes during the activation of PYP (*18, 20, 21*). Large shifts in the pK_a values of the pCA and Glu46 side chain during the PYP photocycle are expected to be of direct importance to this mechanism of PYP receptor activation. The unusually low initial pK_a of the pCA in the pG dark state of PYP creates the potential for light-triggered proton transfer that activates PYP.

Effects on Protein Stability. The contribution of hydrogen bonding to protein stability has been studied in a wide range of proteins. Mutational analysis of the contribution of buried hydrogen bonds to $\Delta G°_U$ has yielded values of ~2 kcal/mol of destabilization per hydrogen bond (*39*−*43*), but this value depends significantly on the structural context of the hydrogen bond (*44*). In the case of the PYP active site, the E46−pCA hydrogen bond is unusually short (*17*), and this ionic hydrogen bond is expected to be significantly strengthened due to the negative charge on the pCA (*45*).

In line with the expected stabilizing effect of the Glu46−pCA hydrogen bond on PYP, 14 of the Glu46 substitutions result in reduced $\Delta G°_U$ values. On the basis of the visible λ_{max} of the E46I, -L, and -V mutants and the volumes of these three side chains, we argued above that the main effect of these substitutions is to remove the active site hydrogen bond between residue 46 and the pCA. The

$\Delta G°_U$ of these three mutants is reduced by 1.0 ± 0.7 kcal/mol, significantly less than expected for the dissociation energy of typical ionic hydrogen bonds. This suggests the existence of compensatory effects involving adjustments in protein structure. The E46D, -K, -P, and -R mutants exhibit a significantly lower $\Delta G°_U$ than the other substitutions, with an average reduction in $\Delta G°_U$ of 4.9 ± 0.8 kcal/mol. For these mutants, additional destabilizing effects based on charge burial and conformational restriction are expected to play a role. These are also the four substitutions with the lowest *m* values, suggesting that they may already be partially unstructured in the native state. Indeed, since the pCA pK_a in these mutants is at or above 8.0, they are likely to be partially acid denatured at the pH of the Gdm-HCl titration, which was performed at pH 8.0, explaining the observed correlation between the values of $\Delta G°_U$ and *m* (Table 1).

The E46A, E46M, and E46W mutants exhibit stabilities higher than anticipated. We propose that the surprising stability of E46W PYP (only 1.5 kcal/mol lower than that of wtPYP) is due to the hydrogen bond between the NH group of the Trp side chain and the pCA indicated by the absorbance spectrum of E46W PYP (Figure 8b). The E46M mutant is slightly more stable than wtPYP, despite the disruption of the E46−pCA hydrogen bond. Methionine residues have two features that may allow them to enhance $\Delta G°_U$. Their unbranched nature makes them highly flexible (*46, 47*) and thus able to pack with other residues easily. Second, the polarizability of the sulfur atom creates the potential for a relatively large London dispersion force interaction. The dispersion energy between a S and CH_2 group in the cysteinyl-tRNA synthetase was estimated to be as high as ~5 kcal/mol (*48*). The unperturbed $\Delta G°_U$ in E46A PYP may be due to an ordered water molecule in the cavity created in the E46A mutant, which hydrogen bonds to the pCA.

Interestingly, the $\Delta G°_U$ correlates with all of the other functional properties measured here: pCA Φ_{fl} and pK_a, λ_{max}, and percentage photobleaching [correlation coefficients of greater than ±0.64 (see Table 1)]. The correlation between $\Delta G°_U$ and Φ_{fl} suggests that a more rigid pCA in a well-packed active site results in both an increased $\Delta G°_U$ and a reduced Φ_{fl}. The detected correlation between $\Delta G°_U$ and the pK_a of the pCA indicates the importance of interactions in the active site for the stability of PYP. The strong pK_a shifts in the pCA and Glu46 indicate that this region of the protein is an "energy hot spot" for the structure of PYP, and this notion is supported by the observed correlation between the stability of PYP and the pK_a of its chromophore. The partial unfolding of the pB state (*33*) triggered by the light-induced electrostatic epicenter (*20*) at this site can explain the correlation between pB lifetime (photobleaching percentage) and the complete unfolding ($\Delta G°_U$) of the protein.

High-Throughput Protein Biophysics of PYP. Science has been progressing toward approaches that are smaller, faster, and higher-throughput. Recently, high-throughput approaches have begun to be applied to quantitative studies of protein biophysics (*49*−*54*). We report the development and utilization of methods for 96-well-based purification and quantitative characterization of PYP and its mutants. This opens the way for high-throughput approaches to quantitative biophysical studies of PYP, and more generally for water-soluble proteins with good expression levels. This approach is applicable to systems that involve a spectroscopic observable (e.g., absorbance, fluorescence) from either the protein itself (e.g., aromatic side chains, cofactors, attached fluorescent probes) or a substrate.

One of the advantages of using the Glu46 position is that it is the most well studied residue in PYP, allowing us to compare our results with those reported in the literature for wtPYP, E46A, E46D, and E46Q based on traditional large-scale purification and spectroscopy methods (see Table S2 of the Supporting Information). We observed very similar absorbance maxima for these samples which have been published (*8, 14*−*16, 36*). Similarly, the pK_a values of these mutants as determined here using microscale methods closely match those reported in the literature (*8, 15, 16, 25, 34*). In summary, with the exception of the kinetics of pG recovery in the E46Q mutant (see above), the microscale data correspond well to the published properties of these four samples (Table S2 of the Supporting Information). This provides a strong validation of the methods developed and used in this study (also see the Discussion in the Supporting Information).

Because of the somewhat reduced purity of the samples obtained by 96-well purification, it is possible that a small percentage of misfolded PYP contributes to the spectroscopic data reported here. This issue would only arise in the case of misfolded PYP that absorbs in the visible region where the photocycle kinetics and titration curves were detected, and where fluorescence was excited. For the acid denaturations and denaturant titrations, this could cause either two distinct transitions or highly anomalous values for the pH titration *n* values and the denaturant *m* values, respectively. These effects are not observed (Figures 4c and 5c). The two measurements most sensitive to a misfolded PYP subpopulation are the kinetics of pG recovery and the pCA Φ_{fl}. Misfolded PYP could give rise to a slow component in the kinetics of pG recovery. Recently, we reported evidence that the isomerization of Pro54 is involved in this slow component (*55*), but a misfolded PYP fraction could increase the contribution of this slow phase. Thus, the relative contributions of the slow phase in the E46X mutants (Figure 6c) should be interpreted with care; the other conclusions reached here are not affected by this issue. An additional complication for the comparison of pG recovery kinetics in the E46X mutants is that the data reported in Figure 6 were determined at one selected pH value (pH 8.0). The kinetics of pG recovery are pH-dependent, and this dependence can be significantly altered in PYP mutants (*8, 56, 57*). The data reported here on pG recovery kinetics in the E46X mutants provide a snapshot of the pB lifetime at one specific pH value.

Misfolded PYP could also cause an increase in pCA Φ_{fl} (Figure 3) that is not representative of the well-folded fraction of the mutant. For the E46H, E46K, and E46Y mutants, we have performed subpicosecond pump−probe spectroscopic measurements using highly purified samples and found that the excited-state lifetime of the mutants correlates well with their Φ_{fl} (A. Philip, R. A. Nome, N. F. Scherer, and W. D. Hoff, unpublished results). This correlation indicates that the pCA Φ_{fl} for these three mutants is not caused by a small percentage of highly fluorescent misfolded PYP but is representative of the bulk of the PYP molecules.

The study reported here provides a test case for the high-throughput biophysical characterization of libraries of mutants. Advantages of this approach over the study of individual mutants are that it allows the rapid identification of (i) trends in the data that link amino acid structure to a functional property (see Figure S4 and the Discussion in the Supporting Information for a cluster analysis of the data reported here), (ii) mutants with atypical behaviors, and (iii) the "evolvability" of selected functional properties and the position of the wild-type protein in the range of values observed for the mutants.

These advantages are illustrated by the following observations. (i) A dependence of both the position of the λ_{max} and the pK_a of the pCA chromophore in PYP was found on the strength of the hydrogen bond between position 46 and the pCA, based on a comparison of the properties of wtPYP with E46Q PYP and the E46I, -L, and -V mutants. (ii) The E46Q mutant has been studied extensively (*8, 14, 17, 20, 21, 35, 57*−*60*) and greatly accelerates the final photocycle step at pH >7 (*8*). Here we find that the E46Q mutant is unusual since it is the only substitution at position 46 that results in such a dramatic acceleration of the photocycle rate. (iii) All of the functional parameters measured here were significantly affected by mutations at position 46, confirming the central position of this residue in tuning a variety of functional properties of PYP. In the case of the pCA Φ_{fl} and pK_a, wtPYP was found to have the lowest values of all 20 side chains, supporting the notion that these two values were functionally optimized during evolution, whereas for the other properties studied this is not the case. The approach reported here opens the way to high-throughput studies of large libraries of mutants of PYP and other soluble chromophoric proteins.

Implications for Proton Transfer and Protein Conformational Changes during the PYP Photocycle. Two key events in the PYP photocycle are pCA protonation and protein conformational changes. Two pathways for proton transfer have been proposed in the literature for the protonation of the pCA chromophore during the PYP photocycle: (i) intramolecular proton transfer from Glu46 to the pCA (*18*−*20*) and (ii) proton transfer from solvent water (*58*). The observation that all of the E46X mutants exhibit a photocycle with a pB intermediate shows that Glu46 is not an essential part of the proton transfer pathway for pCA protonation upon pB formation. The data reported here do not allow a conclusion about the proton transfer pathway in wtPYP.

Three distinct models have been proposed regarding the propagation of conformational changes during the PYP photocycle. First, it has been proposed that the transiently deprotonated side chain of Glu46 functions as an electrostatic epicenter that triggers a large "protein quake" (*18, 20, 21*). In a second model, solvent exposure of the pCA upon isomerization creates a hydrophobic cavity that collapses upon itself, causing a distortion of the protein (*5*). Third, it has been proposed that hydrogen bonding interactions of Asn43 are a key element of the structural pathway that relays conformational changes from the photoactive site to the N-terminal region (*60*). Since all of the 19 substitution mutants studied here have a pB intermediate but do not contain the proposed electrostatic epicenter, its presence is not required for the formation of the blue-shifted photocycle intermediate. However, the protein quake model leads to the prediction that the conformational changes upon formation of this intermediate will be significantly smaller for these mutants. This has indeed been confirmed for E46Q PYP on the basis of time-resolved FTIR (*20*) and NMR (*21*) spectroscopy. No high-throughput measurement for determining the extent of the conformational changes during the PYP photocycle is currently available. Thus, the data reported here do not reveal the extent of the structural changes in the 19 mutants studied here, and the prediction given above remains to be tested in future work.

SUPPORTING INFORMATION AVAILABLE

Supplemental methods provide further details about the 96-well protein purification and data acquisition for PYP. Supplemental discussion is provided on pH titrations, the kinetics of pG recovery, validation of the data, analysis of correlations in the data, and spectral tuning effects. Four figures are included regarding the microscale purification of PYP, analysis of pG recovery kinetics, measured and predicted photobleaching fractions, and hierarchical clustering of the E46X mutants. Two tables list the properties of the 20 E46X samples and a comparison with published data on these mutants. This material is available free of charge via the Internet at http://pubs.acs.org.

REFERENCES

1. Meyer, T. E. (1985) Isolation and characterization of soluble cytochromes, ferredoxins and other chromophoric proteins from the halophilic phototrophic bacterium *Ectothiorhodospira halophila*. *Biochim. Biophys. Acta 806*, 175–183.
2. Meyer, T. E., Yakali, E., Cusanovich, M. A., and Tollin, G. (1987) Properties of a water soluble, yellow protein isolated from a halophilic phototrophic bacterium that has photochemical activity analogous to sensory rhodopsin. *Biochemistry 26*, 418–423.
3. Sprenger, W. W., Hoff, W. D., Armitage, J. P., and Hellingwerf, K. J. (1993) The eubacterium *Ectothiorhodospira halophila* is negatively phototactic, with a wavelength-dependence that fits the absorption spectrum of the photoactive yellow protein. *J. Bacteriol. 175*, 3096–3104.
4. Hellingwerf, K. J., Hendriks, J., and Gensch, T. (2003) Photoactive Yellow Protein, a new type of photoreceptor protein: Will this "yellow lab" bring us where we want to go? *J. Phys. Chem. A 107*, 1082–1094.
5. Cusanovich, M. A., and Meyer, T. E. (2003) Photoactive yellow protein: A prototypic PAS domain sensory protein and development of a common signaling mechanism. *Biochemistry 42*, 4759–4770.
6. Imamoto, Y., and Kataoka, M. (2007) Structure and photoreaction of photoactive yellow protein, a structural prototype of the PAS domain superfamily. *Photochem. Photobiol. 83*, 40–49.
7. Kort, R., Hoff, W. D., Van West, M., Kroon, A. R., Hoffer, S. M., Vlieg, K. H., Crielaard, W., Van Beeumen, J. J., and Hellingwerf, K. J. (1996) The xanthopsins: A new family of eubacterial blue-light photoreceptors. *EMBO J. 15*, 3209–3218.
8. Genick, U. K., Devanathan, S., Meyer, T. E., Canestrelli, I. L., Williams, E., Cusanovich, M. A., Tollin, G., and Getzoff, E. D. (1997) Active site mutants implicate key residues for control of color and light cycle kinetics of photoactive yellow protein. *Biochemistry 36*, 8–14.
9. Hoff, W. D., Düx, P., Hård, K., Devreese, B., Nugteren-Roodzant, I. M., Crielaard, W., Boelens, R., Kaptein, R., Van Beeumen, J., and Hellingwerf, K. J. (1994) Thiol ester-linked *p*-coumaric acid as a new photoactive prosthetic group in a protein with rhodopsin-like photochemistry. *Biochemistry 33*, 13959–13962.
10. Baca, M., Borgstahl, G. E. O., Boissinot, M., Burke, P. M., Williams, D. R., Slater, K. A., and Getzoff, E. D. (1994) Complete chemical structure of photoactive yellow protein: Novel thioester-linked 4-hydroxycinnamyl chromophore and photocycle chemistry. *Biochemistry 33*, 14369–14377.

11. Hoff, W. D., van Stokkum, I. H., van Ramesdonk, H. J., van Brederode, M. E., Brouwer, A. M., Fitch, J. C., Meyer, T. E., van Grondelle, R., and Hellingwerf, K. J. (1994) Measurement and global analysis of the absorbance changes in the photocycle of the photoactive yellow protein from *Ectothiorhodospira halophila*. *Biophys. J. 67*, 1691–1705.
12. Kim, M., Mathies, R. A., Hoff, W. D., and Hellingwerf, K. J. (1995) Resonance Raman evidence that the thioester-linked 4-hydroxycinnamyl chromophore of photoactive yellow protein is deprotonated. *Biochemistry 34*, 12669–12672.
13. Borgstahl, G. E. O., Williams, D. R., and Getzoff, E. D. (1995) 1.4 Å structure of photoactive yellow protein, a cytosolic photoreceptor: Unusual fold, active site, and chromophore. *Biochemistry 34*, 6278–6287.
14. Mihara, K., Hisatomi, O., Imamoto, Y., Kataoka, M., and Tokunaga, F. (1997) Functional expression and site-directed mutagenesis of photoactive yellow protein. *J. Biochem. 121*, 876–880.
15. Devanathan, S., Brudler, R., Hessling, B., Woo, T. T., Gerwert, K., Getzoff, E. D., Cusanovich, M. A., and Tollin, G. (1999) Dual photoactive species in Glu46Asp and Glu46Ala mutants of photoactive yellow protein: A pH-driven color transition. *Biochemistry 38*, 13766–13772.
16. Meyer, T. E., Devanathan, S., Woo, T., Getzoff, E. D., Tollin, G., and Cusanovich, M. A. (2003) Site-specific mutations provide new insights into the origin of pH effects and alternative spectral forms in the photoactive yellow protein from *Halorhodospira halophila*. *Biochemistry 42*, 3319–3325.
17. Anderson, S., Crosson, S., and Moffat, K. (2004) Short hydrogen bonds in photoactive yellow protein. *Acta Crystallogr. D60*, 1008–1016.
18. Xie, A., Hoff, W. D., Kroon, A. R., and Hellingwerf, K. J. (1996) Glu46 donates a proton to the 4-hydroxycinnamate anion chromophore during the photocycle of photoactive yellow protein. *Biochemistry 35*, 14671–14678.
19. Imamoto, Y., Mihara, K., Hisatomi, O., Kataoka, M., Tokunaga, F., Bojkova, N., and Yoshihara, K. (1997) Evidence for proton transfer from Glu-46 to the chromophore during the photocycle of photoactive yellow protein. *J. Biol. Chem. 272*, 12905–12908.
20. Xie, A., Kelemen, L., Hendriks, J., White, B. J., Hellingwerf, K. J., and Hoff, W. D. (2001) Formation of a new buried charge drives a large-amplitude protein quake in photoreceptor activation. *Biochemistry 40*, 1510–1517.
21. Derix, N. M., Wechselberger, R. W., van der Horst, M. A., Hellingwerf, K. J., Boelens, R., Kaptein, R., and van Nuland, N. A. J. (2003) Lack of negative charge in the E46Q mutant of photoactive yellow protein prevents partial unfolding of the blue-shifted intermediate. *Biochemistry 42*, 14501–14506.
22. Kumauchi, M., Hara, M., Stalcup, P., Xie, A., and Hoff, W. D. (2008) Identification of six new photoactive yellow proteins: Diversity and structure-function relationships in a bacterial blue light photoreceptor. *Photochem. Photobiol. 84*, 956–969.
23. Van der Horst, M. A., van Stokkum, I. H., Crielaard, W., and Hellingwerf, K. J. (2001) The role of the N-terminal domain of photoactive yellow protein in the transient partial unfolding during signalling state formation. *FEBS Lett. 497*, 26–30.
24. Kroon, A., Hoff, W. D., Fennema, H., Koomen, G.-J., Verhoeven, J. W., Crielaard, W., and Hellingwerf, K. J. (1996) Spectral tuning, fluorescence, and photoactivity in hybrids of photoactive yellow protein, reconstituted with native or modified chromophores. *J. Biol. Chem. 271*, 31949–31956.
25. Hoff, W. D., Van Stokkum, I. H. M., Gural, J., and Hellingwerf, K. J. (1997) Comparison of acid denaturation and light activation in the eubacterial blue-light receptor photoactive yellow protein. *Biochim. Biophys. Acta 1322*, 151–162.
26. Meyer, T. E., Tollin, G., Hazzard, J. H., and Cusanovich, M. A. (1989) Photoactive yellow protein from the purple phototrophic bacterium *Ectothiorhodospira halophila*. Quantum yield of photobleaching and effects of temperature, alcohols, glycerol, and sucrose on kinetics of photobleaching and recovery. *Biophys. J. 56*, 559–564.
27. Van Brederode, M. E., Gensch, Th., Hoff, W. D., Hellingwerf, K. J., and Braslavsky, S. E. (1995) Photoinduced volume change and energy storage associated with the early transformations of the photoactive yellow protein from *Ectothiorhodospira halophila*. *Biophys. J. 68*, 1101–1109.
28. Meyer, T. E., Tollin, G., Causgrove, T. P., Cheng, P., and Blankenship, R. E. (1991) Picosecond decay kinetics and quantum yield of fluorescence of the photoactive yellow protein from the halophilic purple phototrophic bacterium *Ectothiorhodospira halophila*. *Biophys. J. 59*, 988–991.
29. Braun, P., Hu, Y., Shen, B., Halleck, A., Koundinya, M., Harlow, E., and LaBaer, J. (2002) Proteome-scale purification of human proteins from bacteria. *Proc. Natl. Acad. Sci. U.S.A. 99*, 2654–2659.
30. Imamoto, Y., Ito, T., Kataoka, M., and Tokunaga, F. (1995) Reconstitution photoactive yellow protein from apoprotein and *p*-coumaric acid derivatives. *FEBS Lett. 374*, 157–160.
31. Lee, B.-C., Croonquist, P. A., and Hoff, W. D. (2001) Mimic of photocycle by a protein folding reaction in photoactive yellow protein. *J. Biol. Chem. 276*, 44481–44487.
32. Santoro, M. M., and Bolen, D. W. (1992) A test of the linear extrapolation of unfolding free energy changes over an extended denaturant concentration range. *Biochemistry 31*, 4901–4907.
33. Lee, B.-C., Pandit, A., Croonquist, P. A., and Hoff, W. D. (2001) Folding and signaling share the same pathway in a photoreceptor. *Proc. Natl. Acad. Sci. U.S.A. 98*, 9062–9067.
34. van der Horst, M. A., van Stokkum, I. H. M., Dencher, N. A., and Hellingwerf, K. J. (2005) Controlled reduction of the humidity induces a shortcut recovery reaction in the photocycle of photoactive yellow protein. *Biochemistry 44*, 9160–9167.
35. Sugishima, M., Tanimoto, N., Soda, K., Hamada, N., Tokunaga, F., and Fukuyama, K. (2004) Structure of photoactive yellow protein (PYP) E46Q mutant at 1.2 Å resolution suggests how Glu46 controls the spectroscopic and kinetic characteristics of PYP. *Acta Crystallogr. D60*, 2305–2309.
36. Imamoto, Y., Koshimizu, H., Mihara, K., Hisatomi, O., Mizukami, T., Tsujimoto, K., Kataoka, M., and Tokunaga, F. (2001) Roles of amino acid residues near the chromophore of photoactive yellow protein. *Biochemistry 40*, 4679–4685.
37. Sauer, U. H., Sun, D. P., and Matthews, B. W. (1992) Tolerance of T4 lysozyme to proline substitutions within the long interdomain α helix illustrates the adaptability of proteins to potentially destabilizing lesions. *J. Biol. Chem. 267*, 2393–2399.
38. Peracchi, A. (2001) Enzyme catalysis: Removing chemically 'essential' residues by site-directed mutagenesis. *Trends Biochem. Sci. 26*, 497–503.
39. Fersht, A. R., Shi, J.-P., Knill-Jones, J., Lowe, D. M., Wilkinson, A. J., Blow, D. M., Brick, P., Carter, P., Waye, M. M. Y., and Winter, G. (1985) Hydrogen bonding and biological specificity analysed by protein engineering. *Nature 314*, 235–238.
40. Shirley, B. A., Stanssens, P., Hahn, U., and Pace, C. N. (1992) Contribution of hydrogen bonding to the conformational stability of ribonuclease T1. *Biochemistry 31*, 725–732.
41. Byrne, M. P., Manuel, R. L., Lowe, L. G., and Stites, W. E. (1995) Energetic contribution of side chain hydrogen bonding to the stability of staphylococcal nuclease. *Biochemistry 34*, 13949–13960.
42. Takano, K., Yamagata, Y., Kubota, M., Funahashi, J., Fujii, S., and Yutani, K. (1999) Contribution of hydrogen bonds to the conformational stability of human lysozyme: Calorimetry and X-ray analysis of six Ser → Ala mutants. *Biochemistry 38*, 6623–9662.
43. Pace, C. N., Horn, G., Hebert, E. J., Bechert, J., Shaw, K., Urbanikova, L., Scholtz, J. M., and Sevcik, J. (2001) Tyrosine hydrogen bonds make a large contribution to protein stability. *J. Mol. Biol. 312*, 393–404.
44. Deechongkit, S., Nguyen, H., Powers, E. T., Dawson, P. E., Gruebele, M., and Kelly, J. W. (2004) Context-dependent contributions of backbone hydrogen bonding to β-sheet folding energetics. *Nature 430*, 101–105.
45. Meot-Ner, M. (2005) The ionic hydrogen bond. *Chem. Rev. 105*, 213–284.
46. Bernstein, H. D., Poritz, M. A., Strub, K., Hoben, P. J., Brenner, S., and Walter, P. (1989) Model for signal sequence recognition from amino acid sequence of 54K subunit of signal recognition particle. *Nature 340*, 482–486.
47. O'Neil, K. T., and DeGrado, W. F. (1990) How calmodulin binds its targets: Sequence independent recognition of amphiphilic α-helices. *Trends Biochem. Sci. 15*, 59–64.
48. Fersht, A. R., and Dingwall, C. (1979) Cysteinyl-tRNA synthetase from *Escherichia coli* does not need an editing mechanism to reject serine and alanine. High binding energy of small groups in specific molecular interactions. *Biochemistry 18*, 1245–1249.
49. Edgell, M. H., Sims, D. A., Pielak, G. J., and Yi, F. (2003) High-precision, high-throughput stability determinations facilitated by robotics and a semiautomated titrating fluorometer. *Biochemistry 42*, 7587–7593.

50. Mansoor, S. E., and Farrens, D. L. (2004) High-throughput protein structural analysis using site-directed fluorescence labeling and the bimane derivative (2-pyridyl)dithiobimane. *Biochemistry 43*, 9426–9438.
51. Hamdan, F. F., Audet, M., Garneau, P., Pelletier, J., and Bouvier, M. (2005) High-throughput screening of G protein-coupled receptor antagonists using a bioluminescence resonance energy transfer 1-based β-arrestin2 recruitment assay. *J. Biomol. Screening 10*, 463–475.
52. Mayhood, T. W., and Windsor, W. T. (2005) Ligand binding affinity determined by temperature-dependent circular dichroism: Cyclin-dependent kinase 2 inhibitors. *Anal. Biochem. 345*, 187–197.
53. Zhang, B., Senator, D., Wilson, C. J., and Ng, S. C. (2005) Development of a high-throughput robotic fluorescence-based assay for HsEg5 inhibitor screening. *Anal. Biochem. 345*, 326–335.
54. Aucamp, J. P., Cosme, A. M., Lye, G. J., and Dalby, P. A. (2005) High-throughput measurement of protein stability in microtiter plates. *Biotechnol. Bioeng. 89*, 599–607.
55. Lee, B.-C., and Hoff, W. D. (2008) Proline 54 *trans-cis* isomerization is responsible for the kinetic partitioning at the last-step photocycle of photoactive yellow protein. *Protein Sci. 17*, 1–10.
56. Joshi, C. P., Borucki, B., Otto, H., Meyer, T. E., Cusanovich, M. A., and Heyn, M. P. (2006) Photocycle and photoreversal of photoactive yellow protein at alkaline pH: Kinetics, intermediates, and equilibria. *Biochemistry 45*, 7057–7068.
57. Borucki, B., Otto, H., Joshi, C. P., Gasperi, C., Cusanovich, M. A., Devanathan, S., Tollin, G., and Heyn, M. P. (2003) pH dependence of the photocycle kinetics of the E46Q mutant of photoactive yellow protein: Protonation equilibrium between I1 and I2 intermediates, chromophore deprotonation by hydroxyl uptake, and protonation relaxation of the dark state. *Biochemistry 42*, 8780–8790.
58. Borucki, B., Devanathan, S., Otto, H., Cusanovich, M. A., Tollin, G., and Heyn, M. P. (2002) Kinetics of proton uptake and dye binding by photoactive yellow protein in wild type and in the E46Q and E46A mutants. *Biochemistry 41*, 10026–10037.
59. Anderson, S., Šrajer, V., Pahl, R., Rajagopal, S., Schotte, F., Anfinrud, P., Wulff, M., and Moffat, K. (2004) Chromophore conformation and the evolution of tertiary structural changes in photoactive yellow protein. *Structure 12*, 1039–1045.
60. Rajagopal, S., Anderson, S., Srajer, V., Schmidt, M., Pahl, R., and Moffat, K. (2005) A structural pathway for signaling in the E46Q mutant of photoactive yellow protein. *Structure 13*, 55–63.

BI801730Y